JTTEE5 23:692–707
DOI: 10.1007/s11666-014-0055-8
1059-9630/$19.00 © ASM International

Production of Nanocrystalline Ni-20Cr Coatings for High-Temperature Applications

Manoj Kumar, Harpreet Singh, and Narinder Singh

(Submitted September 9, 2013; in revised form November 20, 2013)

Presynthesized nanocrystalline Ni-20Cr powder was deposited on SA 516 and T91 boiler steels by a high-velocity oxy-fuel spraying process. Ni-20Cr powder was synthesized by the ball milling approach. The high-temperature oxidation behavior of bare and coated samples was then studied under cyclic isothermal conditions at 900 °C for 50 cycles. The kinetics of oxidation was established using weight change measurements for the bare and coated boiler steels. Uncoated and coated samples of T91 steel were exposed to the superheated zone of a power plant boiler at 750 °C under cyclic conditions for 15 cycles. Each cycle consisted of 100 h of heating followed by 1 h of cooling. Attempts were made to study the kinetics of erosion--corrosion using weight change and thickness loss data for the samples. Different characterization techniques were used to study the oxidized and eroded--corroded samples, including x-ray diffraction, scanning electron microscopy/energy-dispersive spectroscopy, and x-ray mapping analyses. The Ni-20Cr alloy powder coating was found to offer excellent oxidation resistance to the base steels and was successful in reducing the weight gain of SA 516 steel by 98.5 % and that of T91 steel by 65 %. The coating was observed to reduce the erosion--corrosion rate of T91 steel by 86 % in terms of thickness loss. This indicates that the investigated nanostructured coating can be a better choice over conventional coating for erosion--corrosion control of boiler tubes.

Keywords boiler steels, coatings, erosion–corrosion, high-temperature oxidation, HVOF spraying, oxide scale

1. Introduction

Boiler tubes of coal-fired steam generating plants are subjected to high-temperature degradation by erosion–corrosion. Several countermeasures have been suggested and investigated to control this high-temperature degradation of tube materials. Amongst them, thermal spray coatings have attracted considerable attention worldwide to control the problem of high-temperature degradation in such applications. Thermal spraying techniques are becoming popular due to their capability to coat almost any material onto almost any substrate (Ref 1-4). Thermal spray coatings can induce desired surface properties without affecting the metallurgical properties of the substrate material and with no or negligible damage to the environment (Ref 5-8).

One of the variants of thermal spraying, namely the high-velocity oxy-fuel (HVOF) spraying process, developed in the 1980s, has gained considerable popularity due to its various attractive properties. HVOF-sprayed coatings have many advantages such as high bond strength, low porosity, and low residual stress (Ref 9, 10). This technique has many applications for wear and corrosion management and dimensional restoration (Ref 9-14). Moreover, the process provides the possibility of on-site application.

Nanostructured coatings, which contain grains or clusters smaller than 100 nm, or layers or filaments of that dimension (Ref 15), have attracted the attention of many investigators owing to their better properties such as hardness, ductility, and corrosion and wear resistance in comparison with conventional coatings (Ref 16-18). Mechanical milling of powders is used to synthesize nanostructured coating materials (Ref 19, 20). Nickel-based alloys possess several attractive properties, such as wear, erosion, and corrosion resistance as well as good thermal conductivity. Due to these properties, nickel-based coatings are frequently considered to control the problem of erosion–corrosion of power plant boilers (Ref 3). The oxidation and corrosion behavior of high-velocity air–fuel (HVAF)-sprayed conventional and nanostructured NiCrC (80 %NiCr-20 %CrC) coatings was studied by Kai et al. (Ref 21) at 550, 650, and 750 °C separately for 160 h. The nanostructured coatings were found to exhibit higher corrosion resistance, which was attributed to their lower porosity and higher grain boundary area. It was suggested that enhanced grain boundary diffusion in nanostructured coatings promotes the formation of denser Cr_2O_3 scale. This work aims to study the high-temperature behavior of nanostructured Ni-20Cr coatings deposited on SA 516 and T91 steel by HVOF spraying. The main objective of the current work is to develop Ni-20Cr nanostructured coatings for boiler

Manoj Kumar and **Harpreet Singh**, School of Mechanical, Materials & Energy Engineering, Indian Institute of Technology Ropar, Rupnagar, Punjab, India; and **Narinder Singh**, Department of Chemistry, Indian Institute of Technology Ropar, Rupnagar, Punjab, India. Contact e-mails: hnr97@yahoo.com and harpreetsingh@iitrpr.ac.in.

Table 1 Nominal chemical composition (wt.%) of SA 516-grade 70 (SA 516) and SA 213-T91 (T91) boiler steels

Type of steel	C	Mn	Si	S	Nb	P	Cr	Mo	V	Ni	Fe
SA 516	0.27	0.93	0.10	0.06	…	0.05	…	…	…	…	Balance
T91	0.07–0.14	0.30–0.60	0.20–0.50	0.14	0.06–0.10	≤ 0.02	8.00–9.50	0.85–1.05	0.18–0.25	≤ 0.40	Balance

applications by the HVOF spraying route, which can offer better high-temperature oxidation and erosion–corrosion resistance in comparison with conventionally used Ni-20Cr alloy coatings. The outcome of this study shall be useful to explore the possible use of the developed coating for boiler applications.

2. Experimental Details

2.1 Substrate Materials

The substrate materials used in the present investigation were SA 516-grade 70 (SA 516) and SA 213-T91 (T91) steels, which are widely used as boiler tube materials in power plants in India. The materials were procured from Cheema Boilers (Pvt.) Limited, Banmajra, Kurali (Punjab), India. The nominal chemical composition of SA 516 and T91 is reported in Table 1.

Specimens with dimensions of 20 × 15 × 5 mm^3 were cut from SA 516 and T91 boiler steels. The specimens were polished using emery papers of 220, 400, 600, 1000, and 1200 grit and 1/0, 2/0, 3/0, and 4/0 grades. Subsequently, the specimens were polished to mirror finish on a cloth-wheel polishing machine using alumina powder suspension.

2.2 Coating Powder

Presynthesized nanocrystalline Ni-20Cr alloy powder having crystallite size of 10 nm was used to coat SA 516 and T91 samples. The alloy powder was prepared by mechanical alloying of Ni powder having average particle size of 74 μm (Loba Chemie, India) and Cr nanopowder having 59 nm average particle size (presynthesized). The chromium nanoparticles were synthesized by mechanical milling. The mechanical alloying/milling was carried out in a planetary ball mill (Fritsch, P-7 premium line). For the Cr nanoparticles, commercially available Cr powder (Sigma Aldrich) having particle size of 5 μm was milled for 60 h at 300 rpm with ball-to-powder ratio of 10:1. The parameters used for ball milling of Ni (80 wt.%) and Cr (20 wt.%) are reported in Table 2. A complete description of the synthesis procedure was reported in an earlier publication by the authors (Ref 22). These parameters were selected after a comprehensive literature review (Ref 23-27) and by performing a number of milling experiments. The average particle size of the Ni-20Cr alloy powder obtained after 20 h of milling was confirmed using a particle size analyzer (Microtrac Bluewave) and found to be 14 μm. The average crystallite size of powder was calculated by Scherrer's formula using the highest-intensity peak and found to be 10 nm. The crystallite size of the powder was further confirmed by transmission electron microscopy (TEM; TECNAI G20), being found to be 10 nm (Ref 22).

Table 2 Parameters used for ball milling of Ni-20Cr powder

Parameter	Value
Ball-to-powder (B:P) weight ratio	10:1
RPM	300
Running time (min):pause time (min)	30:10
Process control agent	Toluene

Table 3 Process parameters for HVOF spraying of Ni-20Cr powder on SA 516 and T91 steels

Process gas	Air
Oxygen flow rate	260 slpm
LPG flow rate	60 slpm
Air flow rate	600 slpm
Spray distance	150 mm
Powder feed rate	35–40 g/min
Fuel pressure	7 kg/cm^2
Oxygen pressure	10 kg/cm^2
Air pressure	6 kg/cm^2

2.3 Coating Deposition

Ni-20Cr alloy powder was deposited on SA 516 and T91 steel specimens at Metallizing Equipment Company Private Limited (MECPL), Jodhpur, India, using HVOF spraying equipment (HIPOJET-2100). The operating gases were oxygen and liquid petroleum gas (LPG). The parameters used in HVOF spraying are reported in Table 3. The polished steel specimens were grit-blasted using Al_2O_3 (grit 60) after polishing. Samples of each steel were coated in a batch of five by fixing them in a fixture. A fixed number of passes of the spray gun over the surfaces was used to achieve a uniform coating thickness on all six sides of the samples.

2.4 Characterization of As-Sprayed Coatings

Surface characterization of as-sprayed specimens was done using x-ray diffraction (XRD) analysis (PANalytical X'Pert-Pro model with Cu K_α radiation). The surface morphology of the as-sprayed samples was studied by scanning electron microscopy (SEM; JEOL, JSM-6610LV) equipped with energy-dispersive spectroscopy (EDS, Oxford). To measure the porosity, surface images of the polished samples were obtained by an optical microscope (Leica DM4000M) fitted with Metallurgical

software (Leica Microsystems, LMW V 3.6.6). Apparent porosity measurements were made using an image analyzer system with MicroCAM 4.1 software (Radical, Ambala, India). Each reported porosity value is the average of ten readings taken from different micrographs of a particular sample. After surface characterization, the samples were sectioned using a high-precision slow-speed diamond cutter (Scientific, Precimet-1). Subsequently, the sectioned samples were mounted in epoxy and polished using emery papers of 220, 400, 600, 1000, and 1200 grit followed by fine polishing with emery papers of 1/0, 2/0, 3/0, and 4/0 grades. Cloth-wheel polishing was carried out to obtain a mirror finish using 0.3-mm diamond paste. The mounted samples were characterized to obtain their cross-sectional morphology and elemental composition using SEM/EDS analysis. Cross-sectional microhardness was measured using a microhardness tester (Wilson, 402MVD) at load of 100 g with dwell period of 10 s. Ten indentations each were performed at distances of 50, 100, 150, 200, and 250 μm from the coating–substrate interface in the coating area along lines parallel to the substrate material. Subsequently, average values of ten indentations were plotted versus distance from the interface.

2.5 High-Temperature Oxidation Studies in Air

Cyclic isothermal air oxidation studies were conducted at 900 °C for 50 cycles in a silicon carbide tube furnace (TGIS, Roorkee, India) fitted with a proportional–integral–derivative (PID) controller and calibrated to ±1 °C. Bare and coated specimens were polished down to 1200 grit emery paper polishing to obtain a similar condition for reaction before being subjected to the oxidation run. The physical dimensions of the specimens were measured using a digital vernier caliper (Mitutoyo, resolution 0.01 mm) to calculate the surface area of the samples. Subsequently, the specimens were washed properly with acetone to remove any contamination and dried in hot air to remove any moisture. Before starting the air oxidation studies, each prepared specimen was kept in an alumina boat and the initial combined weight of the specimen and boat was measured. The alumina boats used for the oxidation study were preheated at a constant temperature of 1200 °C for 10 h to remove any moisture. Then, the boat containing the specimen was placed in the hot zone of the tube furnace, which was preset at a temperature of 900 °C. Each oxidation cycle consisted of 1 h of heating at 900 °C followed by 20 min of cooling in ambient air. Then, the weight change of the specimen along with the boat was measured after each cycle using an electronic balance (Kern, ABT100-5M, sensitivity 0.01 mg). The aim of the cyclic loading was to create accelerated conditions for oxidation testing. Visual observations of the sample with regard to change in color, lustre, spallation tendency of oxide scale, and coating were also made after the end of each cycle. The kinetics of oxidation was established using the weight change data. After exposure for 50 cycles, the oxidized samples were characterized using XRD and SEM/EDS for the surface as well as cross-sectional analysis as per the procedure mentioned in Sect. 2.4. In this study, ''scale'' refers to material present above the steel substrate, which may include oxidized, partially oxidized, or unaffected coating layers plus any other layer found on the surface, as seen from cross-sectional micrographs. This assumption was made because, after exposure, each coating may suffer some internal oxidation to different depths, which is usually not easy to measure.

2.6 Erosion–Corrosion Studies in a Coal-Fired Boiler

The physical dimensions of the coated and uncoated specimens were measured using a digital vernier caliper (Mitutoyo, resolution 0.01 mm) to calculate the surface area of the samples. A hole with 2 mm diameter was drilled in each sample to hang the same in the boiler with the help of Kanthal wire for fireside erosion–corrosion (hereinafter E-C) studies. The samples were hung in boiler I of Guru Gobind Singh Super Thermal Power Plant (GGSSTPP), Ropar (India) through soot blower dummy points at 42 m height from the base of the boiler. The volumetric flow of flue gases in the boiler was around 700 tonnes/h. Flue gases contain 16 % CO_2 and 3 % O_2 by volume. The gas stream contained ash particles. The chemical analysis of the coal is given in Table 4, while that of ash and flue gas inside the boiler is reported in Table 5. This location for the E-C studies lies in the low-temperature superheated zone of the boiler, with temperature of 740 ± 10 °C. This particular location was chosen because it has highly aggressive flow conditions and the power plant has reported severe failures due to erosion. The direction of gas flow is vertically downwards in this zone. It is pertinent to mention that it is not possible to comment on the direction of impingement of the particles in the gas stream, so each of the surfaces receives eroding particles with different impingement angles at various locations. In this sense, the erosion conditions can be regarded as highly randomized with turbulent gas flow. However, it was not possible to monitor this in the given environment. The studies were conducted under cyclic conditions for 15 cycles. Each cycle consisted of 100 h exposure to the boiler environment followed by 1 h of cooling at ambient conditions. The samples were cleaned after cooling using a light hairbrush. Thereafter, the samples were washed with acetone to remove the ash content deposited on the exposed samples as far as

Table 4 Coal analysis data

Constituent	Wt.%
Total moisture (inherent + surface)	10.43
Inherent moisture	7.55
Ash	34.74
Ash on fire basis (actual)	33.64
Volatile metal	21.59
Gross calorific value (GCV) in kcal/kg	4,187
GCV on fire basis in kcal/kg	4,055
Net GCV in kcal/kg	3,834
Unburnt carbon in fly ash	1.35
Unburnt carbon in bottom ash	5.75

Table 5 Chemical analysis of ash and flue gases inside the boiler

Ash		Flue gases (volumetric flow, 231 m^3/s)	
Constituent	**Wt.%**	**Constituent**	**Value relative to flue gases**
Silica	54.70	SO_x	236 mg/m^3
Fe_2O_3	5.18	NO_x	1,004 $\mu g/m^3$
Al_2O_3-Fe_2O_3/Al_2O_3	29.56	CO_2	12–14 %
Calcium oxide	1.48	O_2	5–7 %
Magnesium oxide	1.45	40 % excess air was supplied to the boiler for the combustion of coal	
SO_3	0.23		
Na_2O	0.34		
K_2O	1.35		
Ignition loss	4.31		

possible. Then, the weight change of the specimens was measured after each cycle using an electronic balance (Kern, model ABT100-5M, sensitivity 0.01 mg). However, weight change data alone are not of much use for predicting the E-C behavior in an actual boiler environment, because of the suspected spalling and ash deposition on the samples. Therefore, the extent of E-C was also evaluated by measuring the thickness loss of the samples due to erosion, spalling, or evaporation by determining the difference in thickness of the specimen before and after 1500 h of exposure to the actual boiler environment. The corrosion rate in mm per year was also calculated by measuring the thickness loss of the substrate as $y \times 8{,}760/1{,}500$, where y is thickness in mm. The eroded–corroded samples were characterized using XRD, SEM/EDS, and x-ray mapping for the surface, as well as cross-sectional analysis as per the procedure mentioned in Sect. 2.4.

3. Results and Discussion

3.1 XRD Analysis of As-Sprayed Coatings

The XRD profiles of nanostructured Ni-20Cr-coated SA 516 and T91 steels are shown in Fig. 1a and b, respectively, being very similar to each other. This analysis reveals the presence of Ni as the primary phase and NiO as the secondary phase in both coated steels. The grain size of the coating on SA 516 and T91 steels was found to be 9.4 and 14 nm, respectively. The grain size of the coating was calculated from the width of the high-intensity peak of Ni (Ref 28-31).

3.2 Porosity and Surface Morphology of As-Sprayed Coatings

SEM micrographs of as-sprayed Ni-20Cr coatings on SA 516 and T91 steels, along with the EDS elemental composition (%) at selected points, are shown in Fig. 2a and b, respectively. The microstructure of the Ni-20Cr powder-coated SA 516 steel consists of fully melted splats at several locations, whereas several other locations have unmelted particles, which are severely deformed to give a

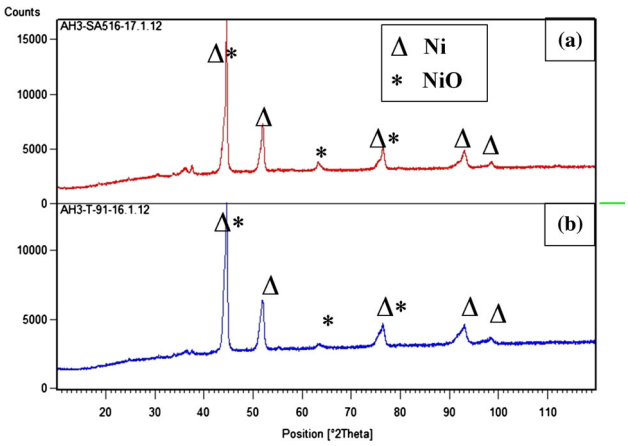

Fig. 1 X-ray diffraction profiles of HVOF-sprayed Ni-20Cr coatings on (a) SA 516 and (b) T91 steels

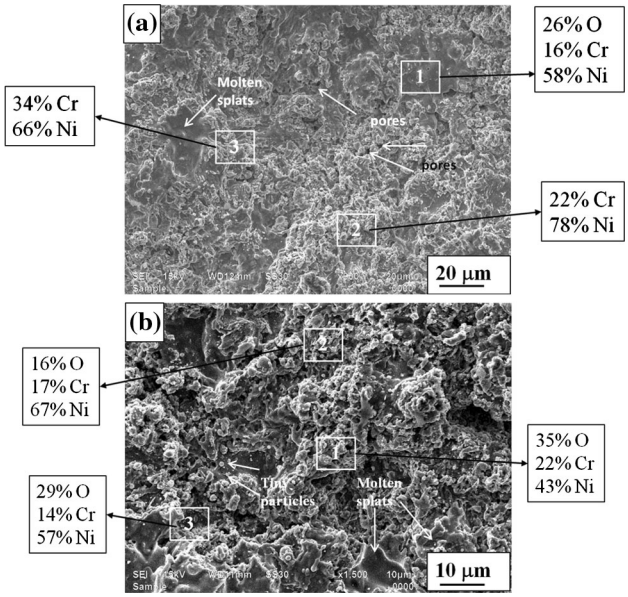

Fig. 2 Surface morphology and SEM/EDS analysis for HVOF-sprayed Ni-20Cr coatings on (a) SA 516 and (b) T91 boiler steels

flattened appearance. Some microvoids are also seen at some locations, giving rise to surface porosity. The average porosity of the coating was found to be 1.65 %. The EDS analysis at some selected points shows dominance of Ni along with Cr as the secondary element in the composition of the coating, approaching the composition of the feedstock powder. There is a significant presence of O at point 1 of the coating, which supports the XRD results regarding the presence of NiO phase in the coating. The SEM micrograph of Ni-20Cr-coated T91 steel shown in Fig. 2b reveals a microstructure consisting of irregularly shaped interlocking splats. There is the presence of fully molten splats at some locations, whereas at some other locations the splat microstructure is flower-like. The average apparent porosity was found to be 1.69 %. Ni and Cr were the main elements along with a significant amount

of O in the coating composition. The presence of oxygen in the coating indicates the possibility of formation of oxides.

3.3 Cross-Sectional Analysis of As-Sprayed Coatings

Cross-sectional SEM backscattered electron imaging (BSEI) of HVOF-sprayed Ni-20Cr coating on SA 516 boiler steel is shown in Fig. 3. The average coating thickness measured from the image was 250 μm. As per standard practice, several passes of the spray gun achieved the required coating thickness over the substrate. This leads to the formation of a lamellar microstructure of thermal spray coatings. The coating in general is dense and has continuous contact with the steel substrate. Cross-sectional line analysis showed the presence of different elements (wt.%) through the thickness of the coating. Ni along with Cr was predominately present in the coating region from line 1 to line 3 with almost uniform concentrations. O was found to be present throughout the coating, indicating the probability of formation of some oxides in the coating microstructure, as also revealed by XRD analysis. Fe was restricted to the steel substrate, without any diffusion into the coating, which is a positive attribute.

A similar analysis of HVOF-sprayed Ni-20Cr coating on T91 boiler steel is shown in Fig. 4. The microstructure by and large was similar to that of the SA 516 steel case. However, the coating–steel interface in this case seemed to have more defects (microvoids) in comparison with the SA 516 case. The average coating thickness as measured from the image was 325 μm. As expected, the coating composition was dominated by nickel in a nearly uniform fashion. Cr was found to be the second most dominant element in the coating. O was present throughout the coating with the exception of line 3 of the cross-section. Near the interface, Fe, Ni, Cr, and O coexisted, indicating interdiffusion of elements of the coating and steel near the interface (Ref 32).

Cross-sectional plots of microhardness versus distance from the coating–substrate interface are shown in Fig. 5. It is obvious from these plots that the variation in microhardness is only marginal in the substrate regions, whereas the variations in hardness are significant in the coating regions. This may be because of anisotropic properties of the thermal spray coatings due to their typical splat structure and directional solidification. The Ni-20Cr coating on SA 516 steel was found to have average microhardness of 522 HV, while the average microhardness of the steel is 186 HV. The corresponding values for the T91 steel case were 463 and 224 HV, respectively. From these data, it is interesting to note that, the softer the steel, the harder the coating produced. This may be attributed to the fact that a softer surface may allow striking particles/splats to deform and stick to the surface more effectively in comparison with a harder surface.

3.4 Cyclic Oxidation Studies

3.4.1 Visual Examination. Macrographs of bare and HVOF-sprayed Ni-20Cr-coated SA 516 and T91 steel

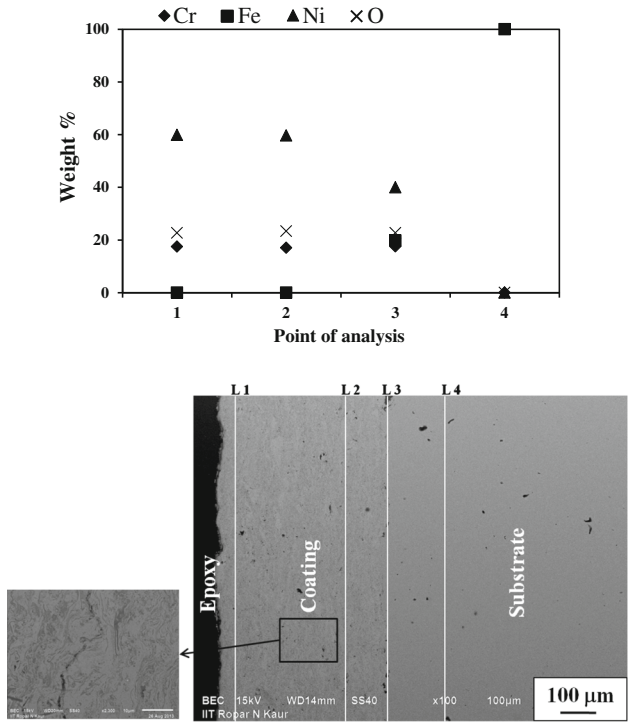

Fig. 3 BSEI and variation of elemental composition across the cross-section of HVOF-sprayed Ni-20Cr coating on SA 516 boiler steel

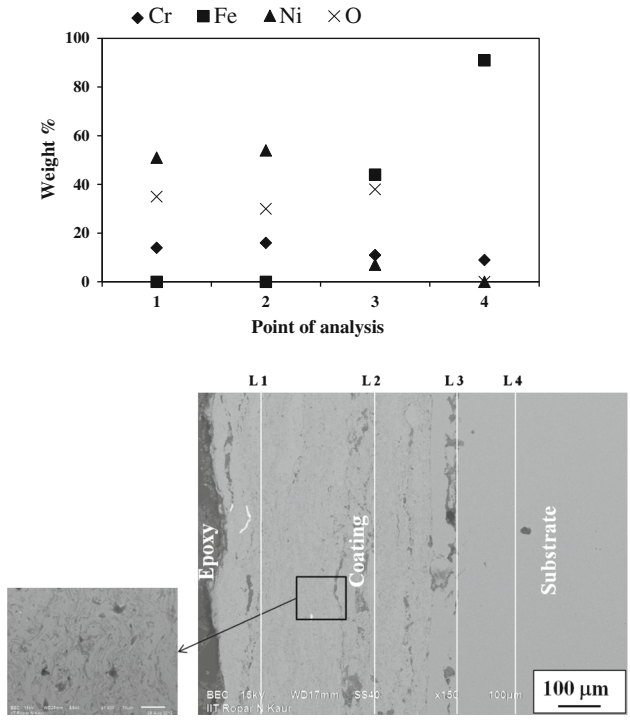

Fig. 4 BSEI and variation of elemental composition across the cross-section of HVOF-sprayed Ni-20Cr coating on T91 boiler steel

specimens before and after exposure to cyclic oxidation in air at 900 °C for 50 cycles are shown in Fig. 6. In the case of bare SA 516 steel, a dark-bluish-color oxide scale was observed on all surfaces after the end of the first cycle. This scale could not be sustained and started separating from the surfaces in the form of flakes. After the 13th cycle, a small crack was observed on one of the surfaces, which started propagating and resulted in delamination of a small layer of oxide scale from the surface by the end of the 15th cycle. This spallation of oxide scale continued until the end of the 50th cycle. Similarly, in the case of bare T91 steel, a dark-grey oxide scale appeared on the surfaces right from the first cycle. The color of the scale did not change subsequently and remained the same until the end of the 50th cycle. The steel showed spalling of scale just after the first cycle, which continued until the end of the exposure. The volume of flakes in the boat increased continuously until the end of the 50 cycles. At the end of the cyclic oxidation study, an irregular and fragile scale was observed on the surfaces of the sample.

The color of the Ni-20Cr-coated SA 516 steel specimen changed to dark grey at the end of the first cycle. The coating was found to remain intact with the steel substrate during the exposure. The coated specimens did not show any spallation, in general, until the end of the 50th cycle, as shown in Fig. 6b-III. In the case of Ni-20Cr-coated T91 steel, the initial color of the sample was dark grey. During the oxidation study, the coating did not show any sign of spallation; however, after the 10th cycle, some superficial microcracks were observed on the sides of the samples. Some of the microcracks showed a tendency to propagate as the exposure time increased. The color of the oxide

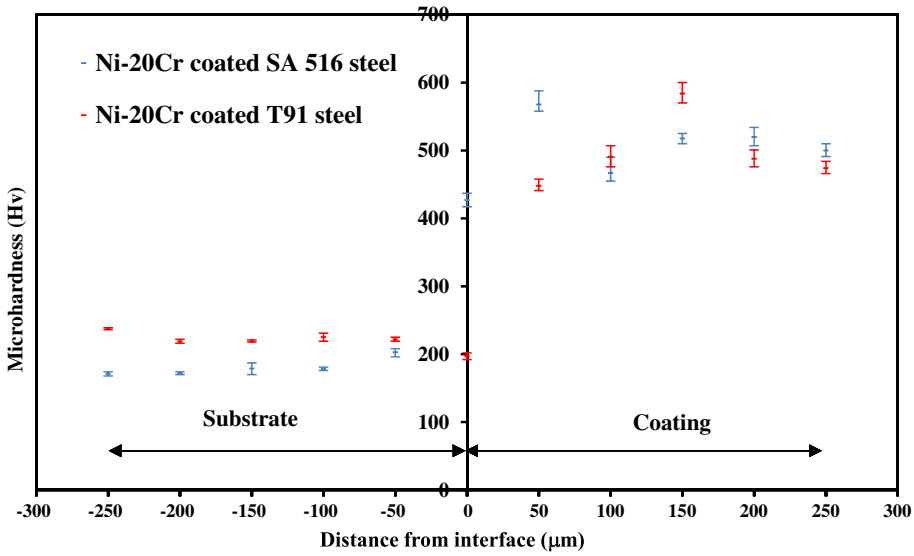

Fig. 5 Cross-sectional microhardness profiles of HVOF-sprayed Ni-20Cr coatings on SA 516 and T91 boiler steels

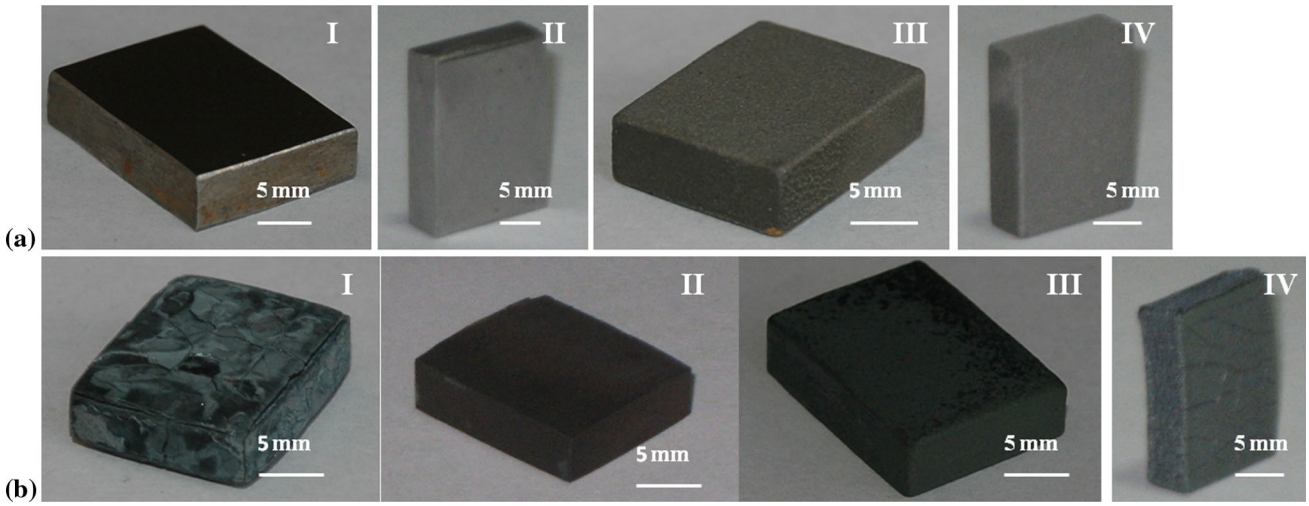

Fig. 6 Macrographs of bare and HVOF-spray-coated boiler steel samples (a) before and (b) after oxidation study at 900 °C for 50 cycles: (I) bare SA 516, (II) bare T91, (III) Ni-20Cr-coated SA 516, and (IV) Ni-20Cr-coated T91

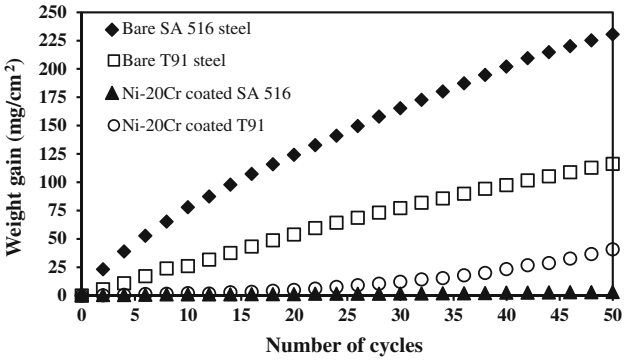

Fig. 7 Plot of weight gain versus number of cycles for bare and HVOF-sprayed Ni-20Cr-coated SA 516 and T91 boiler steels subjected to cyclic oxidation in air at 900 °C for 50 cycles

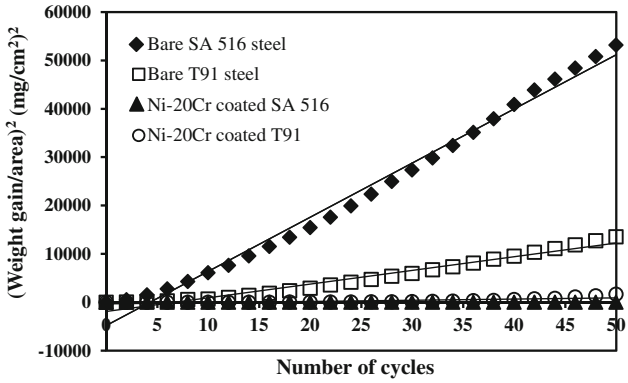

Fig. 8 (Weight gain/area)^2 versus number of cycles for bare and HVOF-sprayed Ni-20Cr-coated SA 516 and T91 boiler steels subjected to cyclic oxidation in air at 900 °C for 50 cycles

scale was found to be dark black at the end of the exposure, as shown in Fig. 6b-IV.

3.4.2 Weight Change Data. Weight change data measured during the high-temperature oxidation study are reported in Fig. 7. The overall weight gain after 50 cycles of air oxidation for the bare SA 516 and T91 steels was found to be 230.5 and 116 mg/cm^2, respectively. Therefore, in terms of weight gain, the T91 steel showed relatively higher air oxidation resistance in comparison with SA 516 steel. In the case of the Ni-20Cr-coated steels, it can be inferred from the plots shown in Fig. 7 that the necessary protection against oxidation was provided, as the oxidation rates were found to be significantly reduced after application of the coating. The weight gains for the Ni-20Cr-coated SA 516 and Ni-20Cr-coated T91 steels were measured to be 2.96 and 40.7 mg/cm^2, respectively. The HVOF-sprayed Ni-20Cr coating could reduce the weight gain of SA 516 and T91 steels by 98.7 and 65 %, respectively, which is a substantial contribution.

Furthermore, plots of (weight change/area)^2 versus number of cycles are shown in Fig. 8, revealing that the bare as well as the coated steel samples, by and large, showed conformance with a parabolic rate law of oxidation, albeit with small deviations. Moreover, the deviations shown by the coated steels were only marginal in comparison with the bare steels. This indicates that the coatings showed a tendency to act as a diffusion barrier to oxidizing species. The parabolic rate constant (K_p) was calculated using a linear least-squares algorithm with a function of the form $(W/A)^2 = K_p t$, where W/A is the weight gain per unit surface area (mg/cm^2) and t is the number of cycles, representing the exposure time. The parabolic rate constants for the bare and coated boiler steels calculated based on exposure data for 50 cycles are presented in Table 6. It is clear from these weight change measurements and parabolic rate constants that the investigated coating offers higher oxidation resistance to SA 516 steel than to T91 steel.

3.5 XRD Analysis of Air-Oxidized Samples

The XRD analysis of the bare and coated samples subjected to cyclic isothermal oxidation in air at 900 °C for 50 cycles is shown in Fig. 9. It is obvious from Fig. 9a and b that the oxide scales of both bare steels contained Fe_2O_3 as the main phase. On the other hand, the analysis of the Ni-20Cr-coated steels indicates the presence of NiO as the main phase (Fig. 9c, d), along with Cr_2O_3 as the secondary phase in the oxide scales.

Table 6 Calculated values of parabolic rate constant (K_p) for the investigated cases

Description	K_p ($\times 10^{-10}$ g^2/cm^4·s)
Bare SA 516 steel	3,109
Bare T91 steel	786
HVOF-sprayed Ni-20Cr-coated T91 steel	68
HVOF-sprayed Ni-20Cr-coated SA 516 steel	0.47

3.6 Surface Scale Morphology

The SEM/EDS analysis of the bare and coated steels subjected to cyclic air oxidation for 50 cycles at 900 °C is shown in Fig. 10. The analysis of the oxidized SA 516 steel indicates the presence of a granular oxide scale with highly oxidized grain boundaries. The EDS analysis (Fig. 10a) reveals that the scale is rich in Fe and O throughout its composition. This indicates the possibility of formation of Fe_2O_3 phase, as also revealed by XRD analysis. Bare T91 steel was observed to have a relatively fine-grained oxide scale with significant presence of microcracks propagating along boundaries, as shown in Fig. 10b. The EDS analysis indicated that the scale is rich in Fe and O throughout its composition along with a noticeable presence of Cr.

The similar analysis of air-oxidized Ni-20Cr-coated SA 516 steel shown in Fig. 10c reveals a scale with a typical pyramidal structure. The EDS analysis indicates a significant concentration of Ni and O in the oxide scale along with small amounts of Cr, indicating the possibility of formation of oxides of Ni and/or Cr. Since the SEM beam penetrates to a lesser depth, Cr indications are low during EDS analysis, but the XRD analysis confirms the formation of oxides of Cr. Since XRD detection reaches relatively greater depths, it is perceptible that Cr oxides may have formed below the outer Ni oxide layers. A

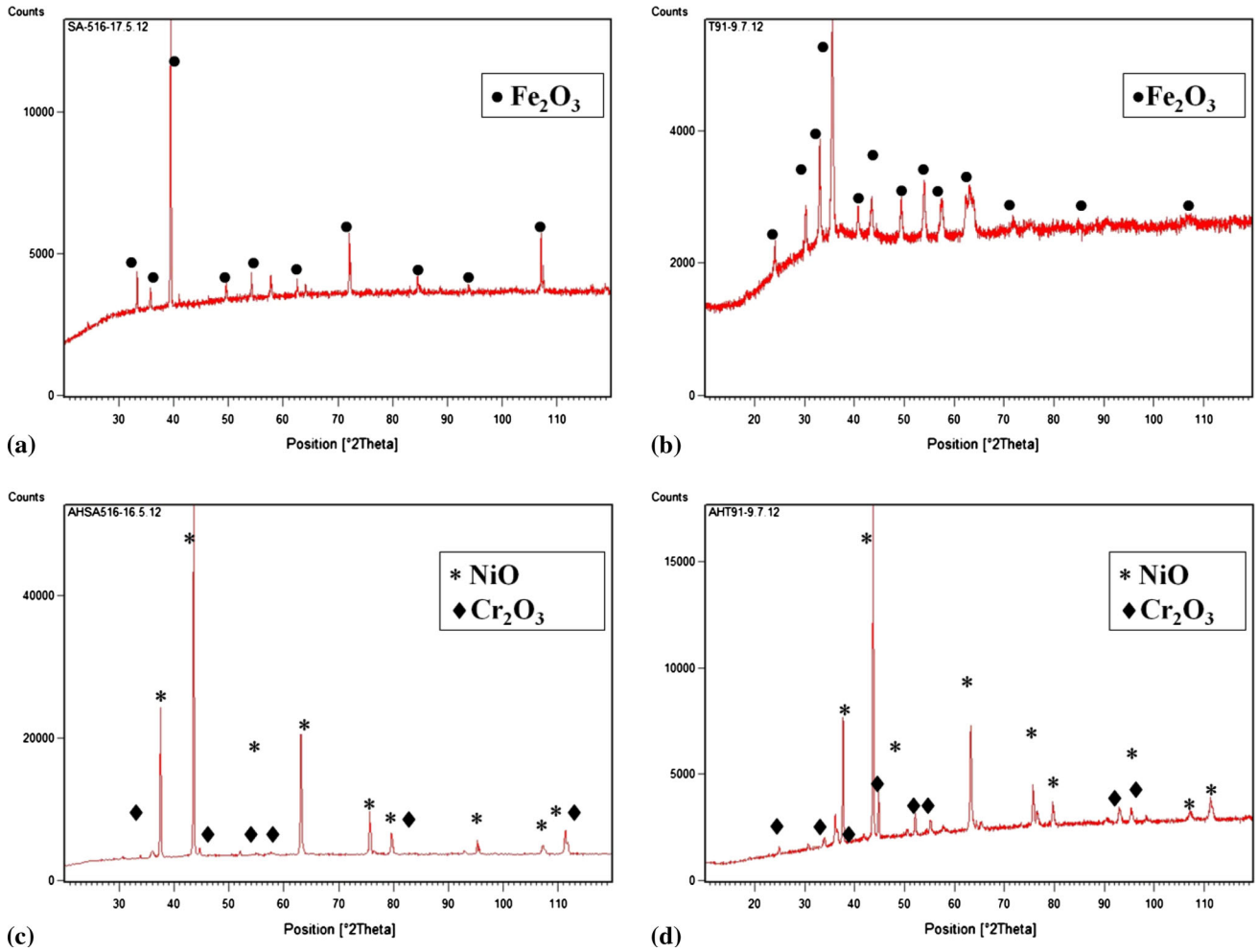

Fig. 9 XRD profiles of bare and HVOF-spray-coated boiler steels subjected to cyclic air oxidation at 900 °C for 50 cycles: (a) bare SA 516, (b) bare T91, (c) Ni-20Cr-coated SA 516, and (d) Ni-20Cr-coated T91 steel

corresponding analysis of Ni-20Cr-coated T91 steel is shown in Fig. 10d, indicating that the scale has a crystalline microstructure typical of NiO phase, as well supported by the EDS measurements at points 2 and 3. Once again, the Cr amounts shown by EDS are only marginal, similar to the SA 516 case. Therefore, it can be concluded that the upper layer (~5 μm) of oxide scale is mainly NiO.

3.7 Cross-Sectional Analysis of Oxidized Samples

3.7.1 Scale Thickness. SEM micrographs of bare and coated samples subjected to cyclic isothermal air oxidation at 900 °C for 50 cycles are presented in Figs. 11–14. A large volume of oxide scale was observed on both bare steel surfaces. The average oxide scale thickness for the oxidized specimens measured from the micrographs is presented in Table 7, as measured at the locations of minimum oxide thickness on the respective samples. The oxide scale thickness for the bare SA 516 steel was greater than that for the bare T91 steel.

3.7.2 Cross-Sectional Scale Morphology. The SEM micrograph for bare SA 516 steel in Fig. 11 shows a thick oxide scale, which has a damaged scale–matrix interface. EDS analysis reveals the presence of Fe and O throughout the scale. The concentrations of Fe and O were found to be uniform from line 1 to line 3, indicating the presence of Fe_2O_3-rich scale. The bare T91 steel was found to have a loose and porous, thicker oxide scale with the presence of lateral cracks parallel to the surface of the steel. The scale was seen to have loose adherence with the matrix (Fig. 12). The composition of the scale was very similar to that of the bare SA 516 steel; that is, the scale was rich in Fe and O.

The SEM micrograph of the oxidized coating on the SA 516 steel (Fig. 13) reveals that the coating retained its identity. It is obvious that the coating successfully retained continuous contact with the steel substrate even after the exposure. EDS analysis revealed the presence of significant amounts of Ni, Cr, and O at the top surface of the scale (lines 1 and 2), which may be responsible for the presence of NiO, Cr_2O_3, and CrO phases in the oxide scale as indicated by XRD analysis. At the interface (line 3) of the scale and substrate, the presence of a large amount of Fe was revealed, along with small amounts of Ni, Cr, and

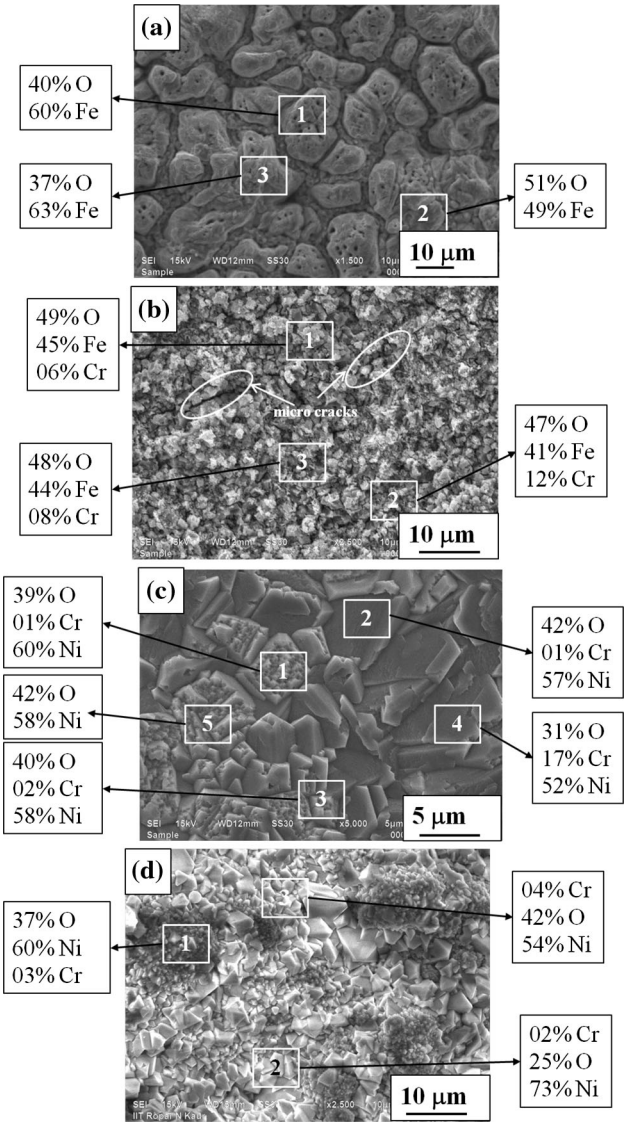

Fig. 10 Surface morphology with EDS analysis for uncoated and HVOF-sprayed boiler steels subjected to cyclic oxidation in air at 900 °C for 50 cycles: (a) bare SA 516 steel, (b) bare T91 steel, (c) Ni-20Cr-coated SA 516 steel, and (d) Ni-20Cr-coated T91 steel

O. The Ni-20Cr coating on the T91 steel also retained its identity and adherence with the steel substrate, as is perceptible from Fig. 14. The upper layers of the scale (line 1 and point 2) were again rich in Ni, O, and Cr.

3.7.3 X-Ray Mappings. Secondary electron imaging (SEI) and x-ray mappings for a part of the oxide scale of the bare SA 516 steel oxidized in air at 900 °C for 50 cycles are shown in Fig. 15. The micrograph of the scale shows the extensive oxidation attack along the scale–steel interface, which resulted in the formation of a loose oxide scale on the steel substrate. The Fe and O mappings indicate that the oxide scale mainly contained iron and oxygen. A similar analysis for a part of the oxide scale of the bare T91 steel oxidized in air at 900 °C for 50 cycles is shown in Fig. 16. The micrograph indicates a badly

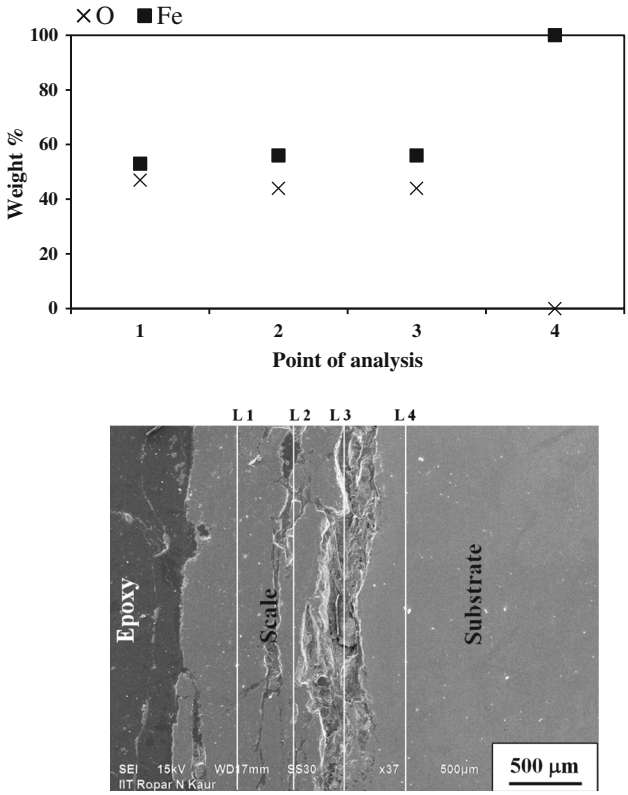

Fig. 11 Oxide scale morphology and variation of elemental composition through the cross-section of bare SA 516 steel subjected to cyclic oxidation in air at 900 °C for 50 cycles

damaged oxide scale, with multiple cracks parallel and normal to the steel surface. The scale mainly contained Fe, Cr, and O. O was present throughout the scale, especially in the center layers of the oxide scale along with Cr.

Secondary electron imaging (SEI) of air-oxidized Ni-20Cr-coated SA 516 steel is shown in Fig. 17. The scale–substrate interface is seen to be free from any cracks or defects. The micrograph indicates a dense scale, which mainly contained nickel and chromium as indicated by the x-ray maps. Oxygen was present throughout the scale. Iron was mainly restricted to the steel substrate, which is indicative of the fact that the coating successfully acted as a diffusion barrier to the elements of the base steel. An analogous analysis of air-oxidized Ni-20Cr-coated T91 steel is shown in Fig. 18. The micrograph shows a dense and intact scale, which mainly contained Ni, Cr, and O. Fe was mainly confined to the base steel.

3.8 E-C Studies in a Coal-Fired Boiler

3.8.1 Weight Change and Thickness Loss Data. The plots of weight change per unit area versus number of cycles for the uncoated and coated steel specimens exposed to the actual boiler environment are shown in Fig. 19. The uncoated T91 steel showed a rapid weight gain until the end of the second cycle. The plot presents a slight decline in weight from the second to third cycle. However, the weight gain accelerates again from the third

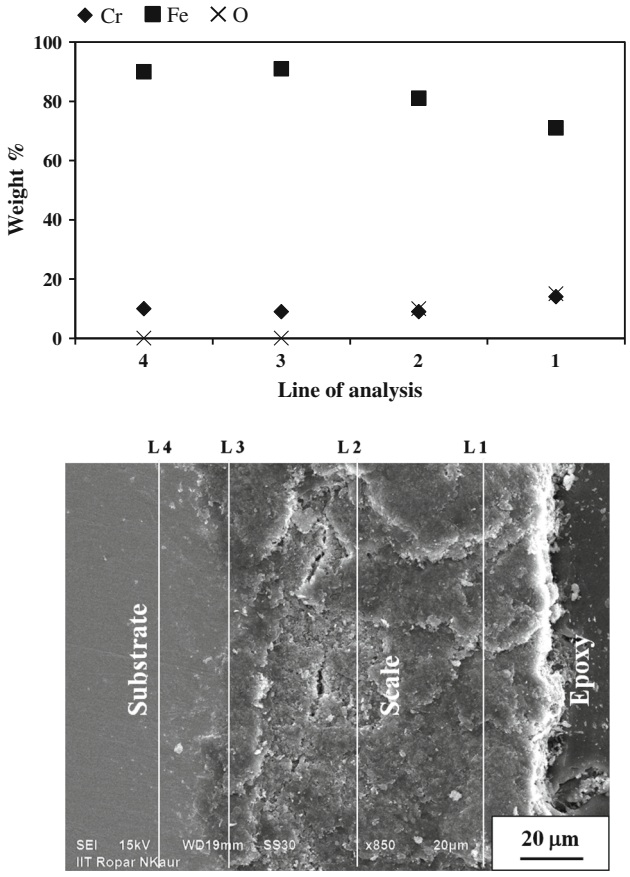

Fig. 12 Oxide scale morphology and variation of elemental composition through the cross-section of bare T91 steel subjected to cyclic oxidation in air at 900 °C for 50 cycles

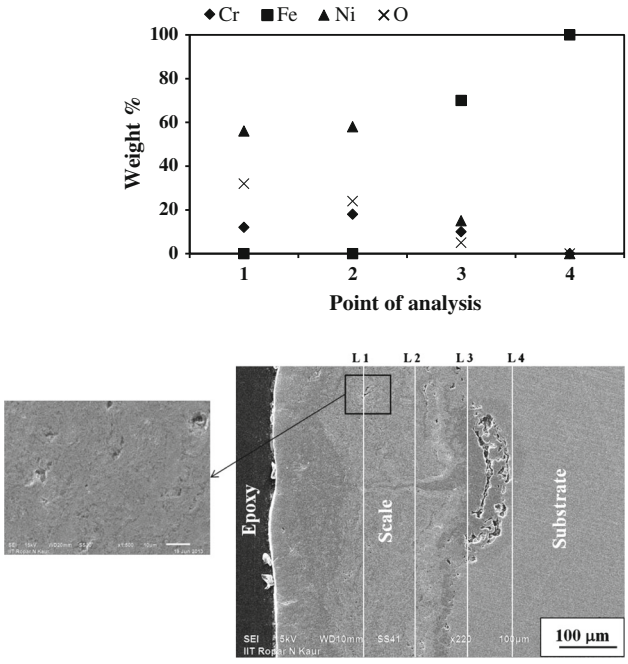

Fig. 13 Oxide scale morphology and variation of elemental composition through the cross-section of HVOF-sprayed Ni-20Cr-coated SA 516 steel subjected to cyclic oxidation in air at 900 °C for 50 cycles

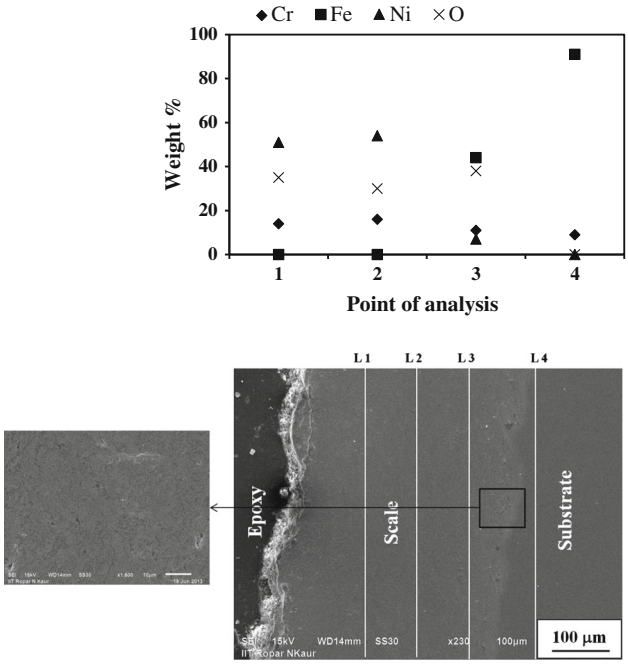

Fig. 14 Oxide scale morphology and variation of elemental composition through the cross-section of HVOF-sprayed Ni-20Cr-coated T91 steel subjected to cyclic oxidation in air at 900 °C for 50 cycles

to the fifth cycle. Subsequently, consistent weight change was observed from the fifth to sixth cycle, and the weight change further accelerated from the sixth to seventh cycle. The weight change again declined slightly from the seventh to eighth cycle, followed by a constant weight change from the eighth to tenth cycle. Then, the weight change accelerated abruptly from the 10th to 11th cycle, followed by a consistent increase in weight change from the 11th to 15th cycle. It is believed that this increase in weight change from the 1st to 2nd cycle, 3rd to 5th cycle, 6th to 7th cycle, and 10th to 15th cycle may be due to the formation and growth of oxide scale. However, the decrease in weight during exposures may be due to erosion, which is observed in the form of spallation of oxide scale during physical observation of the samples. HVOF-sprayed Ni-20Cr-coated T91 exposed to the boiler environment showed an increase in weight change after the first cycle until the end of the third cycle. Further, the plot presents a decline in the weight change during the third to fourth cycle, and subsequently the weight change accelerated from the fourth to eighth cycle. On further exposure, the weight change increased abruptly from the 8th to 9th cycle, and the weight change further decreased slightly during the 9th to 10th cycle and remained consistent from the 10th to 12th cycle. Again, the weight change accelerated from the 12th to 13th cycle, followed by a decline in weight change from the 13th to 14th cycle, and remained constant from the 14th to 15th cycle. The

uncoated T91 steel and coated T91 steel showed an overall weight change of 6.34 and 1.24 mg/cm^2, respectively. The corrosion rate (mm per year) calculated based on the thickness loss data for the uncoated and coated steel was found to be 0.40 and 0.057 mm/year, respectively. It is clear from these corrosion rates that the investigated coating reduced the corrosion rate of the base steel by 86 %.

3.8.2 XRD Analysis. X-ray diffraction (XRD) analysis of the uncoated and coated samples subjected to cyclic E-C study in the actual boiler environment at 740 ± 10 °C for 15 cycles is shown in Fig. 20. Fe_2O_3, Fe_3O_4, Al_2SiO_5, and $FeCr_2O_4$ were identified as the main phases in the scales of bare T91 (Fig. 20a), whereas for the HVOF-sprayed Ni-20Cr-coated T91 steel, oxides such as NiO, Al_2O_3, Cr_2O_3, and SiO_2 were found (Fig. 20b), which are oxides well known for their corrosion resistance. Chatha et al. (Ref 39) observed similar phases during E-C studies of Ni-20Cr-coated T91 steel in the platen superheater zone of a coal-fired boiler.

Table 7 Average scale thickness (μm) for bare and HVOF-sprayed Ni-20Cr-coated boiler steels exposed to cyclic oxidation in air at 900 °C for 50 cycles

Description	Thickness (μm)
Bare SA 516 steel	700
Bare T91 steel	80
Ni-20Cr-coated SA 516 steel	125
Ni-20Cr-coated T91 steel	350

3.9 Discussion

3.9.1 As-Sprayed Coatings. Presynthesized nanocrystalline Ni-20Cr powder could be successfully deposited on SA 516 and T91 boiler steels by a HVOF spray process using the given parameters. The average thickness of the Ni-20Cr coatings deposited on the SA 516 and T91 steels was found to be 250 and 325 μm, respectively. A comparison of the microhardness of the as-sprayed nanostructured Ni-20Cr coatings with their conventional (micron-sized powder coating) counterpart is presented in Table 8. It is evident from this comparison that the investigated coatings showed a 70 % improvement in hardness, which is significant.

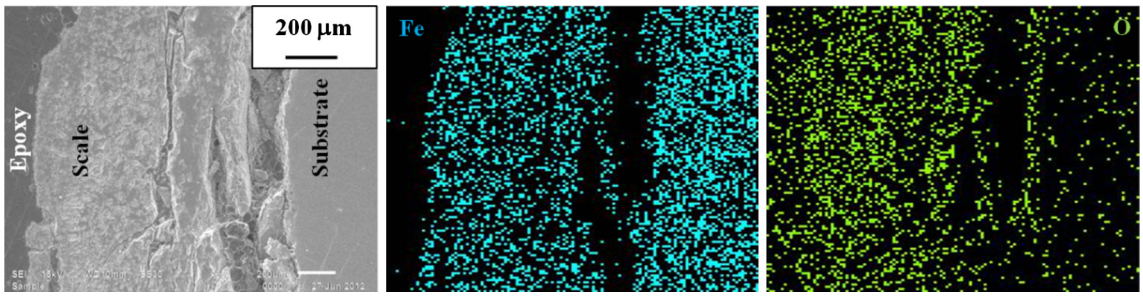

Fig. 15 Secondary electron imaging (SEI) and x-ray mapping of the cross-section of bare SA 516 boiler steel subjected to cyclic oxidation in air at 900 °C for 50 cycles

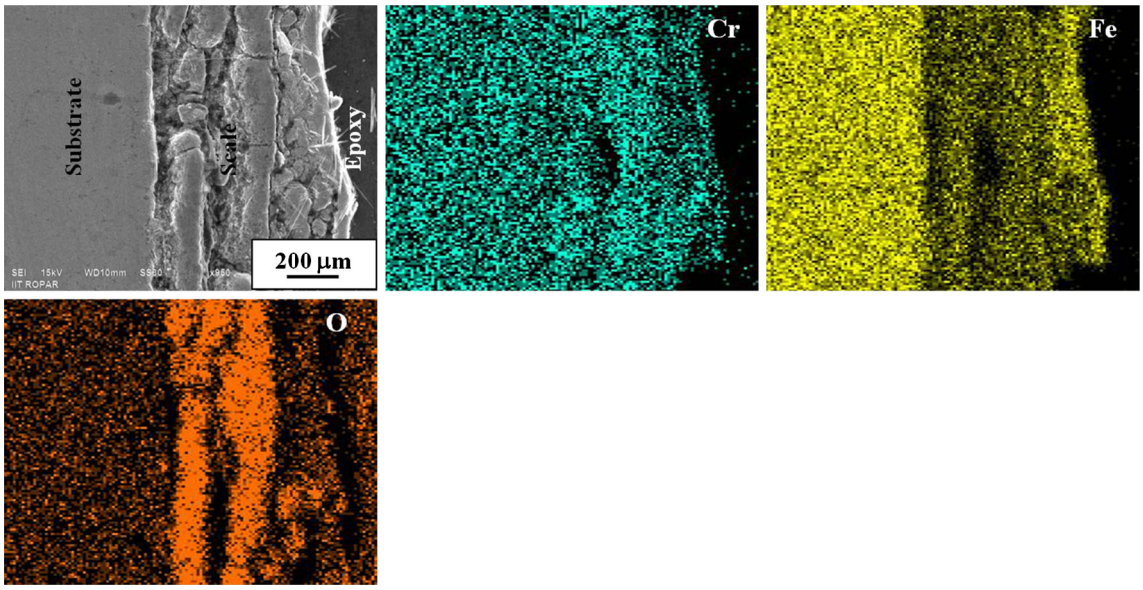

Fig. 16 SEI and x-ray mapping of the cross-section of bare T91 boiler steel subjected to cyclic oxidation in air at 900 °C for 50 cycles

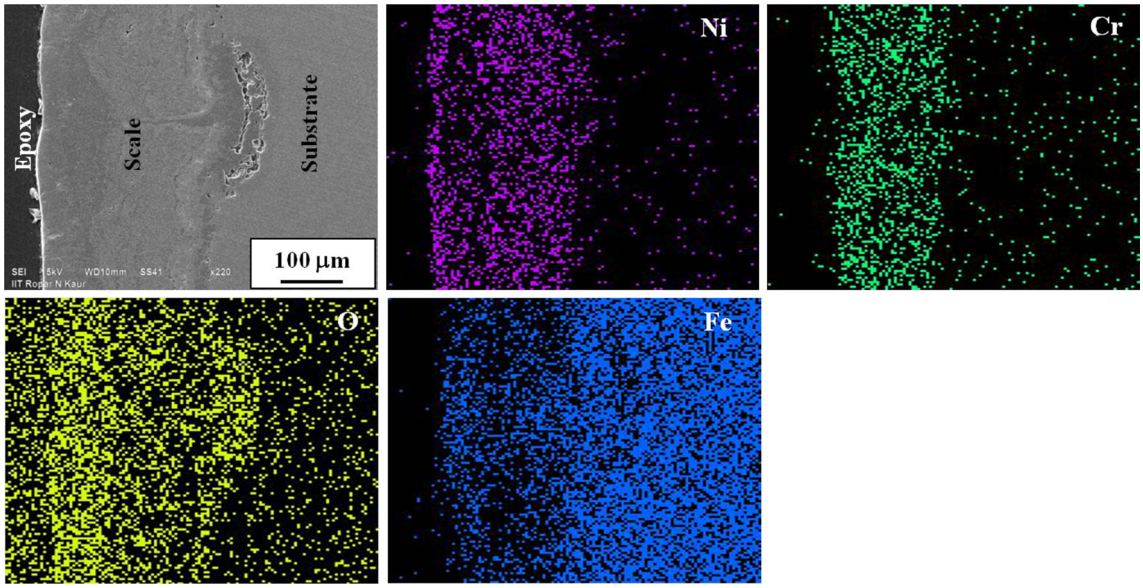

Fig. 17 SEI and x-ray mapping of the cross-section of HVOF-sprayed Ni-20Cr-coated SA 516 boiler steel subjected to cyclic oxidation in air at 900 °C for 50 cycles

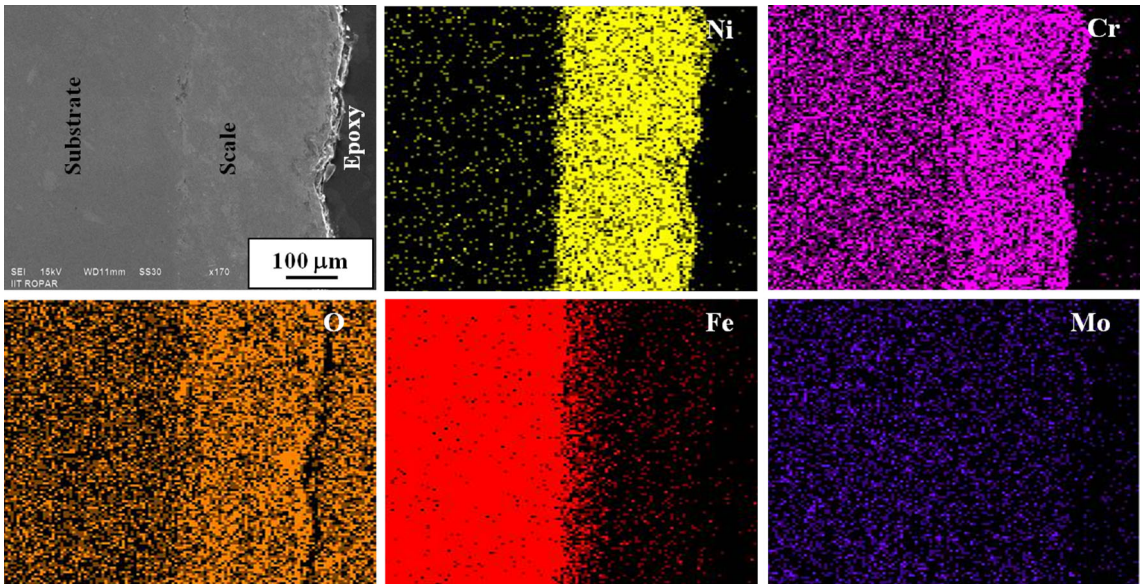

Fig. 18 SEI and x-ray mapping of the cross-section of HVOF-sprayed Ni-20Cr-coated T91 boiler steel subjected to cyclic oxidation in air at 900 °C for 50 cycles

These improved microhardness values of the nanostructured coatings may be attributed to the high density and refinement in grain size of the feedstock powder due to mechanical milling. The higher microhardness of the coatings in comparison with the steel substrates may be due to the typical splat structure, the cohesive strength of the individual splats because of the high impact velocity of the coating particles, and directional solidification (Ref 33).

The coating exhibited a dense and intact microstructure, with splats (lamellae) oriented parallel to the substrate surface as shown in Fig. 3a, b. The lamellae parallel to the substrate provide the necessary protection against corrosive species penetrating towards the steel substrate (Ref 34). The observed NiO in the coatings may have formed due to in-flight oxidation during the spraying process and/or have preexisted in the feed material. The XRD results for the as-sprayed coatings are well supported by the surface as well as cross-sectional SEM/EDS analyses.

3.9.2 Air-Oxidation Studies. The SA 516 and T91 steels showed extensive spalling of their oxide scales, and

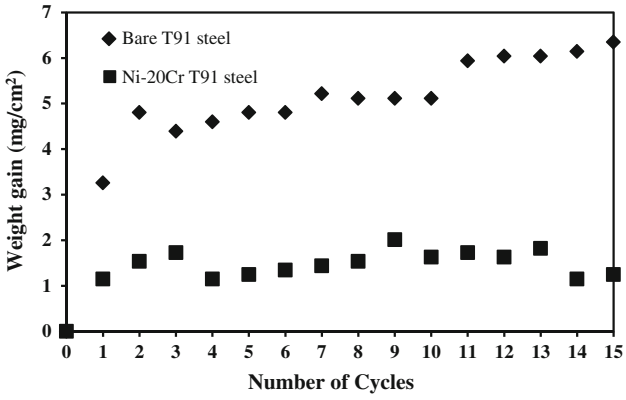

Fig. 19 Weight gain versus number of cycles for uncoated and HVOF-sprayed Ni-20Cr-coated T91 boiler steel subjected to the actual boiler environment at 750 °C for 15 cycles

the weight gain was substantial after exposure to air oxidation at 900 °C for 50 cycles, as shown in Fig. 6. A similar weight change trend and extensive spallation following a parabolic rate law of oxidation were observed by Bala et al. (Ref 35) for SA 516 steel and by Gonda et al. (Ref 36) for T91 steel. After deposition of the HVOF-sprayed Ni-20Cr nanocrystalline coating, the oxidation rates of the given steels were significantly reduced. This may be due to the formation of denser oxide scale due to enhanced grain boundary diffusion (Ref 37, 38). Comparison of the air-oxidation data of the investigated Ni-20Cr-coated SA 516 steel with its conventional (micron-sized powder coating) counterpart (Ref 35) shows that both coatings have comparable overall weight gain after 50 cycles. In this sense, the nanocrystallinity of the coating is not useful to enhance the oxidation performance of the coating. However, the investigated coating on the

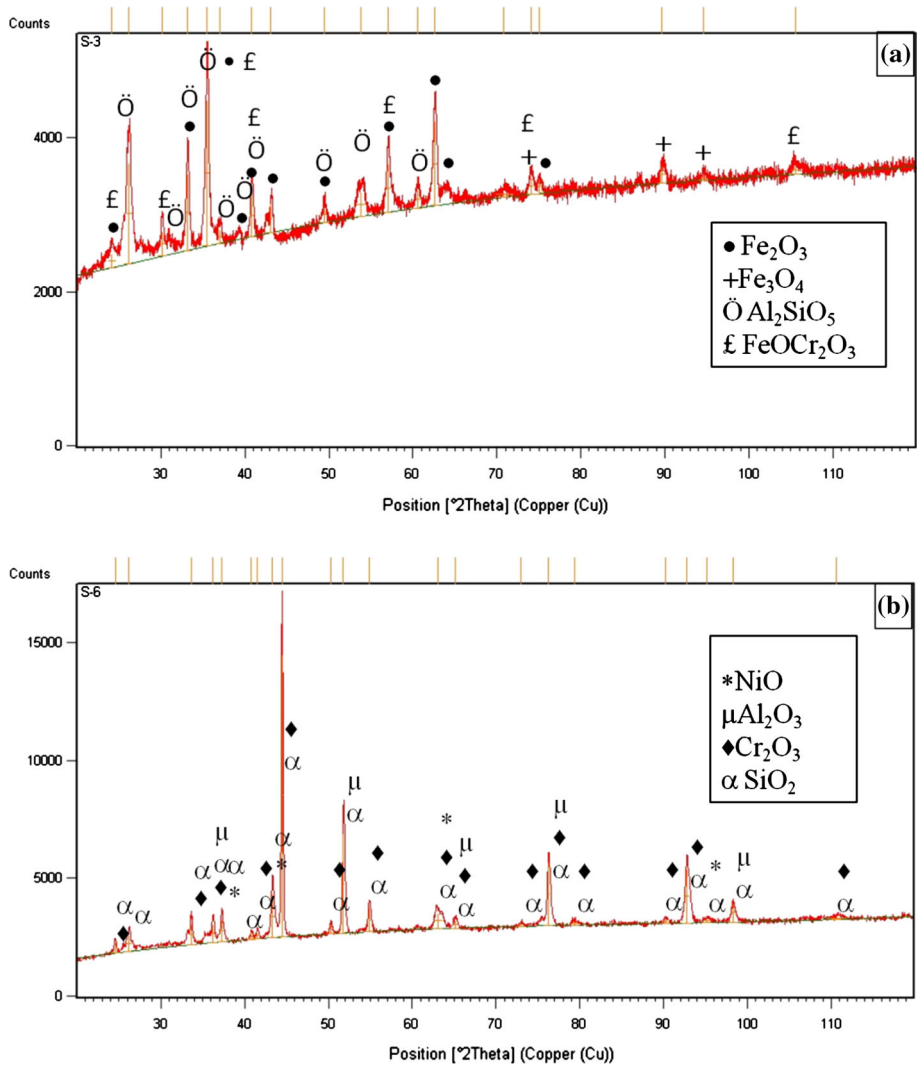

Fig. 20 X-ray diffraction profiles of uncoated and HVOF-spray-coated boiler steel subjected to an actual boiler environment at 750 °C for 15 cycles: (a) uncoated T91 steel and (b) Ni-20Cr-coated T91 steel

Table 8 Comparison of developed nanostructured Ni-20Cr coating with conventional Ni-20Cr coating on different boiler steels

S. no.	Description of coating/substrate	Average microhardness		Improvement (%)
		Conventional coating, HV	Nanostructured coating, HV	
1.	Ni-20Cr/SA 516	300 (Ref 35)	522	70
2.	Ni-20Cr/T91	270 (Ref 39)	463	70

SA 516 steel showed higher oxidation resistance in comparison with the coated T91 steel. This may be attributed to the fact that the coating on SA 516 exhibited defect-free contact with the steel substrate (Fig. 3) in comparison with the T91 steel (Fig. 4). This difference in interface intactness can be further explained on the basis of the different hardness of the base steels. It is a well-established fact that microstructural features, especially the coating–substrate interface, play a major role in controlling oxidation.

Surface XRD analysis indicated the formation of Fe_2O_3 as the main constituent in the top scale in both bare steels after high-temperature cyclic air oxidation at 900 °C. These results were further supported by the SEM/EDS analysis. EDS analysis of the cross-section showed the presence of Fe along with O along the outer layer in the case of the oxidized SA 516 steel. A small amount of Cr was also seen along with Fe and O along the outer layer of the oxidized T91 steel, which may be due to the presence of an adequate amount of Cr in the steel. The XRD analysis of the Ni-20Cr-coated SA 516 and T91 steels revealed the presence of protective oxides of Ni and Cr in the scale. These results were further supported by surface SEM/EDS and cross-sectional point analysis. X-ray mappings also supported the presence of these elements. The EDS analysis indicated a significant concentration of Ni and O along with a small amount of Cr in the oxide scales of both coated steels. This may be due to the fact that the SEM beam penetrates to a lesser depth, so Cr indications were low during EDS analysis, but XRD analysis confirmed the formation of oxides of Cr. Since XRD detection reaches relatively greater depths, it is perceptible that Cr oxides may have formed below the outer Ni oxide layers. This observation was further supported by the respective x-ray mappings (Figs. 17, 18).

The oxide scale showed poor adhesion on the bare SA 516 and T91 boiler steel samples, but it was found to be intact on the coated SA 516 and T91 steels. The calculated parabolic rate constants (K_p) followed the order: bare SA 516 steel > bare T91 steel > coated T91 steel > coated SA 516 steel, as shown in Table 6, indicating that the coating was successful in reducing the oxidation rates of the steels. Further, it was found that the nanostructured Ni-20Cr coating decreased the oxidation rate of SA 516 and T91 steels by 98.7 and 65 %, respectively, which may be attributed to the presence of slowly growing phases such as NiO and Cr_2O_3 in the oxide scale. The presence of these phases is well supported by the surface as well as cross-sectional SEM/EDS analyses.

3.9.3 E-C Studies. Bare T91 steel showed an overall weight gain in the actual boiler environment, as discussed in Sect. 3.8. This may be due to fast-forming Fe_2O_3, Fe_3O_4, Al_2SiO_5, and $FeCr_2O_4$ oxides in its scale, which are usually voluminous and give rise to greater weight gains. The effect of erosion may be perceived from the fact that the specimen showed weight loss during some cycles. This weight loss may be due to erosion caused by harder fly-ash particles. It is perceptible that, as the oxide scale continues to grow thicker, the adherence between its adjacent layers reduced. This makes the scale prone to fail by the impact of eroding particles. This predicted phenomenon is proposed on the basis of the sudden weight reductions after the second and seventh cycles. Therefore, the erosion–corrosion phenomenon for the T91 steel is dictated by cyclic formation and erosion of the oxide scale. The Ni-20Cr coatings exposed to the boiler environment for 15 cycles were found to remain intact with the steel substrates, and no cracks or damage was observed. Fluctuations in the weight change, similar to the bare steel, were also observed for the coated samples, but the extent and frequency of these fluctuations were much lower in the latter case. This again represents the occurrence of corrosion–erosion cycles as discussed for T91 steel. However, the significantly greater hardness of the coatings resulted in significantly lower erosion of coated T91 steel in comparison with uncoated T91 steel. Based on the thickness loss data, the corrosion rates (mm per year) for the uncoated and coated T91 steel were 0.40 and 0.057 mm/year, respectively. So, the coating was found to offer excellent erosion–corrosion resistance to base T91 steel and reduced the corrosion rate by 86 %. Comparison of the corrosion rate of the investigated nanostructured Ni-20Cr coating (0.057 mm/year) with its conventional (micron-sized powder coating) counterpart (0.138 mm/year) (Ref 39) shows that the reduction of the corrosion rate by the former coating is higher in comparison with the latter. This indicates that the investigated nanostructured coating can be a better choice over conventional coating for erosion–corrosion control of boiler tubes. The XRD analysis (Fig. 20b) revealed the formation of Al_2O_3, NiO, and Cr_2O_3 phases on the eroded–corroded HVOF-sprayed Ni-20Cr nanostructured coating. Out of these phases, Al_2O_3 corresponds to the ash particles, whereas NiO and Cr_2O_3 oxides may have formed by oxidation of the coating. The Cr_2O_3 phase is said to be a thermodynamical stable phase up to very high temperatures due to its very high melting point and forms dense, continuous, and adherent layers that inhibit interaction of oxygen with the underlying coating/substrate (Ref 40). Moreover, Cr_2O_3 oxide has a significantly high hardness in comparison with Fe-based alloys. Based on the above discussion, it

may be concluded that the nanocrystalline Ni-20Cr coating can provide significant high-temperature protection to T91 steel in actual boiler conditions. Evaluation of the erosion–corrosion performance of the coating on SA 516 steel is under progress.

4. Conclusions

1. Presynthesized nanocrystalline Ni-20Cr alloy powder was successfully deposited on SA 516 and T91 boiler steels by a HVOF spray process. The thickness of the coating achieved was 250 and 325 μm, respectively, for SA 516 and T91 steels. The coatings were found to be nanostructured.
2. The coatings were found to have lamellar splat-like microstructure with an intact coating–substrate interface. HVOF-sprayed Ni-20Cr coatings were found to have significantly higher microhardness (in the range of 463–522 HV) in comparison with SA 516 and T91 steels. The coatings were found to have nearly 70 % greater hardness in comparison with their conventional counterparts.
3. The HVOF-sprayed Ni-20Cr coating on the SA 516 steel was helpful in reducing the overall weight gain (oxidation rate) of the steel by 98 %, whereas a corresponding reduction of 65 % was achieved for the T91 steel. The Ni-20Cr coating was found to be successful in retaining its surface contact with the steel substrates during the entire cycles of experimentation.
4. The investigated Ni-20Cr coating was successful in reducing the thickness loss of the T91 steel by 86 % in an actual boiler environment. Moreover, the investigated nanostructured coating was found to perform better than its conventional micron-sized counterpart.
5. The presence of Cr_2O_3 along with NiO in the scales might have provided better oxidation and erosion–corrosion resistance to the coated steels.

Acknowledgments

Harpreet Singh et al. thankfully acknowledge the research grant from the Department of Science and Technology, New Delhi, India (SR/S3/MERC/023/2010) for carrying out the R&D work on ''Surface engineering to control erosion–corrosion of steam generating plants by nano-particle coatings.''

References

1. R.C. McCune, A.N. Papyrin, J.N. Hall, W.L. Riggs, and P.H. Zajchowski, *Advances in Thermal Spray Science and Technology*, C.C. Berndt and S. Sampath, Eds., ASM International, Materials Park, OH, 1995, vol. 1
2. L. Pawlowski, *The Science and Engineering of Thermal Spray Coatings*, Wiley, New York, 2008
3. J.R. Davis, *A.I.T.S.S.T. Committee, Handbook of Thermal Spray Technology*, ASM International, Materials Park, OH, 2004
4. H. Singh, *Plasma Spray Coatings for Superalloys: Characterization and High Temperature Oxidation Behavior*, VDM Verlag, Saarbrücken, 2009
5. K.L. Choy, Chemical Vapor Deposition of Coatings, *Prog. Mater. Sci.*, 2003, **48**, p 57-170
6. M.A. Young, Health Hazards of Electroplating, *J. Occup. Environ. Med.*, 1965, **7**, p 348-352
7. J.A. Koropchak and S.B. Roychowdhury, Evidence for Aerosol Ionic Redistribution Within Aerosols Produced by Chrome Electroplating, *Environ. Sci. Technol.*, 1990, **24**, p 1861-1863
8. W.T. Tsai, H.P. Chen, and W.Y. Hsien, A Review of Uses, Environmental Hazards and Recovery/Recycle Technologies of Perfluorocarbons (PFCs) Emissions from the Semiconductor Manufacturing Processes, *J. Loss Prev. Process Ind.*, 2002, **15**, p 65-75
9. L. Fedrizzi, S. Rossi, R. Cristel, and P.L. Bonora, Corrosion and Wear Behaviour of HVOF Cermet Coatings Used to Replace Hard Chromium, *Electrochim. Acta*, 2004, **49**, p 2803-2814
10. L. Gil and M.H. Staia, Microstructure and Properties of HVOF Thermal Sprayed NiWCrBSi Coatings, *Surf. Coat. Technol.*, 1999, **120-121**, p 423-429
11. J.C. Tan, L. Looney, and M.S.J. Hashmi, Component Repair Using HVOF Thermal Spraying, *J. Mater. Process. Technol.*, 1999, **92-93**, p 203-208
12. V.V. Sobolev, J.M. Guilemany, and J. Nutting, *High Velocity Oxy-Fuel Spraying—Theory, Structure-Property Relationships and Applications*, Maney Publishing for IOM3, The Institute of Materials, Minerals and Mining, London, 2004
13. J. Stokes, *The Theory and Application of the HVOF Thermal Spray Process*, Dublin City University, Dublin, 2005
14. E. Lugscheider, C. Herbst, and L. Zhao, Parameter Studies on High Velocity Oxy-Fuel Spraying of MCrAlY Coatings, *Surf. Coat. Technol.*, 1998, **108-109**, p 16-23
15. R.W. Seigel, Nanostructured Materials—Mind Over Matter, *Nanostruct. Mater.*, 1993, **3**(1-6), p 1-18
16. J. He and J.M. Schoenung, Nanostructured Coatings, *Mater. Sci. Eng. A*, 2002, **336**, p 274-319
17. T. Grosdidier, A. Tidu, and H.L. Liao, Nanocrystalline Fe-40Al Coating Processed by Thermal Spraying of Milled Powder, *Scripta Mater.*, 2001, **44**, p 387-393
18. B.R. Marple, J. Voyer, J.F. Bisson, and C. Moreau, Thermal Spraying of Nanostructured Cermet Coatings, *J. Mater. Process. Technol.*, 2001, **117**, p 418-423
19. D.B. Witkin and E.J. Lavernia, Synthesis and Mechanical Behavior of Nanostructured Materials via Cryomilling, *Prog. Mater. Sci.*, 2006, **51**, p 1-60
20. J. He and J.M. Schoenung, Nanocrystalline Ni Coatings Strengthened with Ultrafine Particles, *Metall. Mater. Trans. A*, 2003, **34**, p 673-683
21. T. Kai, Z.X. Lin, C. Hua, and Z.J. Shan, Oxidation and Hot Corrosion Behaviors of HVAF-Sprayed Conventional and Nanostructured NiCrC Coatings, *Trans. Nonferrous Met. Soc. China*, 2009, **19**, p 1151-1160
22. M. Kumar, H. Singh, and N. Singh, Synthesis and Deposition of Ni-20Cr Powder Using Cold Spraying, *Surf. Eng.*, 2013, **29**(6), p 419-426
23. C. Suryanarayana, Nanocrystalline Materials, *Int. Mater. Rev.*, 1995, **40**(2), p 41-44
24. M.K. Datta, S.K. Pabi, and B.S. Murty, Phase Fields of Nickel Silicides Obtained by Mechanical Alloying in the Nanocrystalline State, *J. Appl. Phys.*, 2000, **87**(12), p 8393-8400
25. S.S. Nayak, S.K. Pabi, and B.S. Murty, High Strength Nanocrystalline L12-Al3(Ti,Zr) Intermetallic Synthesized by Mechanical Alloying, *Intermetallics*, 2007, **15**, p 26-33
26. S. Varalakshmi, M. Kamaraj, and B.S. Murty, Processing and Properties of Nanocrystalline CuNiCoZnAlTi High Entropy Alloys by Mechanical Alloying, *Mater. Sci. Eng. A*, 2010, **527**, p 1027-1030
27. S.K. Pabi and B.S. Murty, Synthesis of Nanocrystalline Alloys and Intermetallics by Mechanical Alloying, *Bull. Mater. Sci.*, 1996, **19**(6), p 939-956

28. H.P. Klug and L.E. Alexander, *X-Ray Diffraction Procedures*, 2nd ed., Wiley, New York, 1974
29. B.E. Warren, *X-Ray Diffraction*, Dover, New York, 1990
30. H.G. Jiang, M. Ruhle, and E.J. Lavernia, On the Applicability of the X-Ray Diffraction Line Profile Analysis in Extracting Grain Size and Microstrain in Nanocrystalline Materials, *J. Mater. Res.*, 1999, **14**(2), p 549-559
31. T. Chraska, ''TEM Studies of Microstructures and Interfaces of Zirconia Produced by Plasma Spraying,'' Ph.D. Thesis, State University of New York at Stony Brook, NY, USA, 1999
32. J.R. Nicholls, Designing Oxidation-Resistant Coatings, *JOM*, 2000, **52**, p 28-35
33. R.C. Tucker Jr., *Handbook of Deposition Technologies for Films & Coatings*, R.F. Bunshah, Ed., Noyes/William Andrew, LLC, Park Ridge, NJ/Norwich, NY, 1994
34. S. Kamal, R. Jayaganthan, and S. Prakash, High Temperature Oxidation Studies of Detonation-Gun-Sprayed Cr_3C_2-NiCr Coating on Fe- and Ni-Based Superalloys in Air Under Cyclic Condition at 900 °C, *J. Alloy. Compd.*, 2009, **472**, p 378-389
35. N. Bala, ''Investigations on the Hot Corrosion Behaviour of Cold Spray and HVOF Spray Coatings on T22 and SA 516 Steels'', PhD Thesis, Mechanical Engineering Department, Punjab Technical University, Jalandhar, India, 2010
36. D. Gonda, V. Chawla, D. Puri, and S. Prakash, Oxidation Studies of T-91 and T-22 Boiler Steels in Air at 900°C, *J. Miner. Mater. Charact. Eng.*, 2010, **9**(8), p 749-761
37. X. Peng, J. Yan, Y. Zhou, and F. Wang, Effect of Grain Refinement on the Resistance of 304 Stainless Steel to Breakaway Oxidation in Wet Air, *Acta Mater.*, 2005, **53**, p 5079-5088
38. G. Chen and H. Lou, Oxidation Kinetics of Sputtered Ni-5Cr-5Al Nanocrystalline Coating at 900°C and 1000°C, *Nanostruct. Mater.*, 1999, **11**, p 637-641
39. S.S. Chatha, H.S. Sidhu, and B.S. Sidhu, High-Temperature Behavior of a NiCr-Coated T91 Boiler Steel in the Platen Superheater of Coal-Fired Boiler, *J. Therm. Spray Technol.*, 2013, **22**(5), p 838-847
40. F.H. Scott, Principles of Growth and Adhesion of Oxide Scales, *The Role of Active Elements in the Oxidation Behavior of High Temperature Metals and Alloys*, E. Lang, Ed., Elsevier Applied Science, London, 1998